



ELSEVIER

journal homepage: [www.intl.elsevierhealth.com/journals/cmpb](http://www.intl.elsevierhealth.com/journals/cmpb)

# Generalized rough fuzzy c-means algorithm for brain MR image segmentation

Zexuan Ji<sup>a,b,\*</sup>, Quansen Sun<sup>a</sup>, Yong Xia<sup>b,c</sup>, Qiang Chen<sup>a</sup>, Deshen Xia<sup>a</sup>, Dagan Feng<sup>b,d,e</sup>

<sup>a</sup> School of Computer Science and Technology, Nanjing University of Science and Technology, Nanjing, 210094, China

<sup>b</sup> Biomedical and Multimedia Information Technology (BMIT) Research Group, School of Information Technologies, The University of Sydney, NSW 2006, Australia

<sup>c</sup> School of Computer Science, Northwestern Polytechnical University, Xi'an 710072, China

<sup>d</sup> Center for Multimedia Signal Processing (CMSP), Department of Electronic & Information Engineering, Hong Kong Polytechnic University, Hong Kong

<sup>e</sup> Med-X Research Institute, Shanghai JiaoTong University, Shanghai 200025, China

## ARTICLE INFO

### Article history:

Received 21 February 2011

Received in revised form

21 September 2011

Accepted 23 October 2011

### Keywords:

Brain magnetic resonance image

Image segmentation

Intensity inhomogeneity

Fuzzy c-means algorithm

Rough set

Rough-fuzzy c-means algorithm

## ABSTRACT

Fuzzy sets and rough sets have been widely used in many clustering algorithms for medical image segmentation, and have recently been combined together to better deal with the uncertainty implied in observed image data. Despite of their wide spread applications, traditional hybrid approaches are sensitive to the empirical weighting parameters and random initialization, and hence may produce less accurate results. In this paper, a novel hybrid clustering approach, namely the generalized rough fuzzy c-means (GRFCM) algorithm is proposed for brain MR image segmentation. In this algorithm, each cluster is characterized by three automatically determined rough-fuzzy regions, and accordingly the membership of each pixel is estimated with respect to the region it locates. The importance of each region is balanced by a weighting parameter, and the bias field in MR images is modeled by a linear combination of orthogonal polynomials. The weighting parameter estimation and bias field correction have been incorporated into the iterative clustering process. Our algorithm has been compared to the existing rough c-means and hybrid clustering algorithms in both synthetic and clinical brain MR images. Experimental results demonstrate that the proposed algorithm is more robust to the initialization, noise, and bias field, and can produce more accurate and reliable segmentations.

© 2011 Elsevier Ireland Ltd. All rights reserved.

## 1. Introduction

Magnetic resonance (MR) imaging has several advantages over other medical imaging modalities, including the high contrast among different soft tissues, relatively high spatial resolution across the entire field of view and multi-spectral characteristics. Segmentation of brain MR images into gray matter (GM),

white matter (WM) and cerebrospinal fluid (CSF) plays an important role in both clinical practice and neuroscience studies, and hence has attracted extensive research attention.

One of the major difficulties faced by brain MR image segmentation is the bias field in MR images [1,2], which arises from the imperfections in the radio-frequency coils or problems associated with the acquisition sequences. The bias field, also referred to as the intensity non-uniformity (INU), often

\* Corresponding author at: School of Computer Science and Technology, Nanjing University of Science and Technology, Nanjing, 210094, China. Tel.: +86 13913036590.

E-mail address: [jizexuan@hotmail.com](mailto:jizexuan@hotmail.com) (Z. Ji).

0169-2607/\$ – see front matter © 2011 Elsevier Ireland Ltd. All rights reserved.

doi:[10.1016/j.cmpb.2011.10.010](https://doi.org/10.1016/j.cmpb.2011.10.010)

appears as the variation of intensities from the same tissue type over the locations in an image. Usually, the bias field correction and image segmentation are required to be interleaved in an iterative process such that they can benefit from each other to yield better results. Many segmentation approaches with bias field correction have been proposed for brain MR images in the literature [3–6]. Among them, fuzzy clustering based algorithms [7–10] are one of the most popular groups.

Fuzzy c-mean (FCM) clustering has been widely used in medical image segmentation. In FCM, the membership function can handle the overlapped clusters efficiently [11]. However, FCM is known to be vulnerable to outliers. Recently, rough sets have also been incorporated into the c-means framework for image segmentation [12–15]. The resultant rough c-means (RCM) [12] algorithms deal with the uncertainty, vagueness and incompleteness in data [16] via modeling clusters in terms of the upper and lower approximations. The lower approximation is the set of objects that definitely belong to a vague cluster, and the upper approximation is the set of objects that possibly belong to that cluster. However, defining the lower and upper approximations for each cluster is very difficult, and currently relies on the initialization of cluster centroids. An inappropriate initialization may result in less accurate segmentation.

Both fuzzy sets and rough sets provide a mathematical framework to deal with the uncertainties associated with the human cognition process [17]. The membership function of fuzzy sets can handle overlapping partitions; whereas the lower and upper approximations of rough sets can characterize the vagueness and incompleteness in class definition. Therefore, hybrid algorithms, which use fuzzy sets and rough sets in a combined manner, have been proposed [18–21]. However, there are three major disadvantages in these hybrid approaches. First, all data are grouped into rough regions by using a single threshold. Since the threshold is computed based on the highest and second highest memberships of each pixel, the performances of existing hybrid algorithms are very sensitive to the initial cluster prototypes. Second, the weighting parameter that plays a critical role in balancing the contribution of data from positive region and boundary region is set manually. Ideally, this weight should be adaptive to the accuracy of the positive region of each cluster, taking a large value for accurate positive regions and a small value otherwise. Third, each partition is represented by three parameters, including a cluster centroid, a crisp lower approximation and a fuzzy boundary. However, not all pixels can be assigned to the upper approximation. These drawbacks not only prevent existing hybrid algorithms from providing fully automated segmentation, but also decrease their segmentation accuracy.

To overcome these drawbacks, we propose a generalized rough-fuzzy c-means (GRFCM) algorithm to segment brain MR images into GM, WM, CSF and background. In this algorithm, we use a linear combination of orthogonal polynomials from Ref. [22] to approximate the bias field, and incorporate the bias field correction into the clustering process. Thus, the proposed algorithm can be used to segment brain MR images with intensity inhomogeneity. For each cluster, we partition an image into three rough regions, including the positive region, boundary region and negative region [23], with two thresholds. The construction of rough regions can be treated an initialization

step in each iteration of the algorithm. The membership of a pixel belonging to each cluster is estimated with respect to the rough region, in which the pixel lies. Only those pixels in the positive region and boundary region have non-zero memberships, and are used to determine the mean of each cluster. In this way, we improve the accuracy of the cluster estimation and the robustness against initializations. Moreover, the weighting parameter that balances the contribution of each rough region is estimated automatically in our algorithm. Therefore, the proposed algorithm has three major advantages, including the automated estimation of most involved parameters, robustness to the initialization, noise and bias field, and improved segmentation accuracy. The performance of our algorithm has been compared to several clustering-based segmentation algorithms in both synthetic and clinical brain MR images. Note that part of results in this paper was reported in our recent conference paper [24].

## 2. Background

### 2.1. Bias field formulation

The bias field in a brain MR image can be modeled as a multiplicative component of an observed image, shown as follows:

$$I = b \cdot J + n \quad (1)$$

where  $I$  is the measured image,  $J$  is the true image to be restored,  $b$  is an unknown bias field, and  $n$  is the additive zero-mean Gaussian noise. The goal of bias field correction is to estimate the bias field  $b$  from the measured image  $I$  and eliminate it.

Ideally, in the region of tissue  $c$ , the true image  $J$  takes the same value  $v_c$ , which is determined by the measured physical property of that tissue. This property, in conjunction with the spatially coherent nature of each tissue's distribution, implies that the true image  $J$  is approximately a piecewise constant map [7]. Without loss of generality, the bias field  $b$  can be assumed to vary slowly in the entire image domain, and be approximated by a linear combination of bases functions. Theoretically, such approximation can achieve arbitrary accuracy with a sufficiently large number of bases [22].

### 2.2. Rough set

The rough set theory aims to approximate an imprecise concept in the domain of discourse by using a pair of exact concepts, called the lower and upper approximations. Let  $U \neq \emptyset$  be a universe of discourse, an equivalence relation  $R$  defined in it can lead to a partition of  $U$ , denoted by  $U/R = \{X_1, X_2, \dots, X_n\}$ , where each subset  $X_c$  is called a category and represents an equivalence class of  $R$ . Approximation is used to represent the roughness of knowledge. The  $R$ -upper and  $R$ -lower approximations of the subset  $X$  are defined as

$$\begin{cases} \overline{R}X = \cup\{Y \in U/R | Y \cap X \neq \emptyset\} \\ \underline{R}X = \cup\{Y \in U/R | Y \subseteq X\} \end{cases} \quad (2)$$

The lower approximation contains all subsets that are certainly included in  $X$ , and the upper approximation contains all subsets that are possibly included in  $X$ . Based on both approximations, the R-positive, R-negative and R-boundary regions of  $X$  can be defined as follows [23]:

$$\begin{cases} \text{POS}_R(X) = \underline{R}X \\ \text{NEG}_R(X) = U - \bar{R}X \\ \text{BN}_R = \bar{R}X - \underline{R}X \end{cases} \quad (3)$$

### 2.3. Rough-fuzzy c-means clustering

To classify the data set  $\{d_1, d_2, \dots, d_n\}$  into  $C$  clusters, the hybrid rough fuzzy c-means (RFCM) clustering algorithm proposed by Mitra and Pal [19] minimizes the following objective function

$$J_{RFCM} = \begin{cases} \omega \times A_1 + \tilde{\omega} \times B_1 & \text{if } \underline{R}(v_c) \neq \emptyset, \quad B(v_c) \neq \emptyset \\ A_1 & \text{if } \underline{R}(v_c) \neq \emptyset, \quad B(v_c) = \emptyset \\ B_1 & \text{if } \underline{R}(v_c) = \emptyset, \quad B(v_c) \neq \emptyset \end{cases} \quad (4)$$

with

$$\begin{cases} A_1 = \sum_{c=1}^C \sum_{I_i \in \underline{R}(v_c)} \|d_i - v_c\|^2 \\ B_1 = \sum_{c=1}^C \sum_{I_i \in B(v_c)} u_{ci}^m \|d_i - v_c\|^2 \end{cases} \quad (5)$$

where  $v_c$  is the mean pixel value of cluster  $c$ ,  $u_{ci} \in [0, 1]$  is the membership of data  $d_i$  belonging to cluster  $c$ , and the parameters  $\omega$  and  $\tilde{\omega} = (1 - \omega)$  balance the relative importance of lower approximation and boundary region. In this algorithm, cluster  $c$  is characterized by its lower approximation  $\underline{R}(v_c)$ , upper approximation  $\bar{R}(v_c)$  and boundary region  $B(v_c) = \{\bar{R}(v_c) - \underline{R}(v_c)\}$ . For each cluster, all data are grouped into either  $\underline{R}(v_c)$  or  $B(v_c)$  by using a threshold  $\delta$ , which determines the size of granules of rough-fuzzy clustering and hence plays an important role in the RFCM algorithm. Since the threshold  $\delta$  is computed based on the highest and second highest memberships of each pixel, the performance of the RFCM algorithm are very sensitive to the initial cluster prototypes.

## 3. GRFCM algorithm

### 3.1. Objective function

An observed brain MR image with  $N$  pixels is denoted by a data set  $I = \{I_1, I_2, \dots, I_N\}$ , where  $I_i$  is the value of pixel  $i$ . With the bias field model given in Eq. (1), the observed image  $I$  is assumed to be a true signal  $J$  degenerated by the bias field  $b = \{b_1, b_2, \dots, b_N\}$  and zero-mean Gaussian noise  $n$ . Based on the rough theory, the image is further assumed to be partitioned into the positive region  $P(v_c)$ , boundary region  $B(v_c)$  and negative region  $N(v_c)$  for each cluster  $c$ . Segmentation of the observed

brain MR image into  $C$  clusters can be solved by minimizing the following objective function.

$$\begin{aligned} J_{GRFCM} = & \lambda_1 \sum_{c=1}^C \sum_{i \in P(v_c)} u_{ci}^m \|I_i - b_i v_c\|^2 + \lambda_2 \sum_{c=1}^C \sum_{i \in B(v_c)} u_{ci}^m \|I_i - b_i v_c\|^2 \\ & + \lambda_3 \sum_{c=1}^C \sum_{i \in N(v_c)} u_{ci}^m \|I_i - b_i v_c\|^2 \end{aligned} \quad (6)$$

where  $\lambda_1, \lambda_2$  and  $\lambda_3$  are weighting parameters, representing the relative importance of three rough-fuzzy regions and satisfying the constraint  $\lambda_1 + \lambda_2 + \lambda_3 = 1$ .

### 3.2. Rough-fuzzy region determination

For each cluster, three rough-fuzzy regions are determined by using two thresholds, which are estimated based on the distances between each pixel value  $I_i$  and each intensity level  $g_j$  appeared in the image. To reduce the influence of noise, all intensities in the neighborhood of each pixel are used to calculate this distance, shown as follows:

$$d_i(g_j) = \frac{\sqrt{\sum_{k \in \eta_i} (I_k - g_j)^2 / |\eta_i|}}{l_{\max} - l_{\min}}, \quad j = 1, 2, \dots, L \quad (7)$$

where  $\eta_i$  is a neighborhood of pixel  $i$ ,  $|\eta_i|$  is the cardinality of  $\eta_i$ ,  $l_{\max}$  is the maximum intensity,  $l_{\min}$  is the minimum intensity, and  $L$  is the total number of intensity levels in the image. Thus, we have a distance vector  $d_i = \{d_i(g_1), d_i(g_2), \dots, d_i(g_L)\}$  for each pixel  $i$ . Given the maximum  $d_{i,\max}$  and minimum  $d_{i,\min}$  of the vector  $d_i$ , two thresholds can be estimated as follows:

$$\begin{cases} t_1 = \frac{1}{n} \sum_{i=1}^n d_{i,\min} \\ t_2 = \frac{1}{n} \sum_{i=1}^n d_{i,\max} \end{cases} \quad (8)$$

To determine three rough regions for each class  $c$ , we must calculate  $d_i(v_c)$ , the distance between each pixel  $i$  and the mean pixel value of class  $c$ , by using the Eq. (7). Then, the positive region  $P(v_c)$ , boundary region  $B(v_c)$  and negative region  $N(v_c)$  can be obtained by comparing the distance  $d_i(v_c)$  and those two thresholds

$$I_i \in \begin{cases} P(v_c) & \text{if } d_i(v_c) \leq t_1 \\ B(v_c) & \text{if } t_1 \leq d_i(v_c) \leq t_2 \\ N(v_c) & \text{if otherwise} \end{cases} \quad (9)$$

The definition of three rough-fuzzy regions is illustrated in Fig. 1. It is shown that the positive region  $P(v_c)$  gives the lower approximation of cluster  $c$ , and negative region  $N(v_c)$  gives the complement of the higher approximation of cluster  $c$ . Therefore, all data in the positive region  $P(v_c)$  certainly belong to cluster  $c$ , and their membership to cluster  $c$  should be one. All

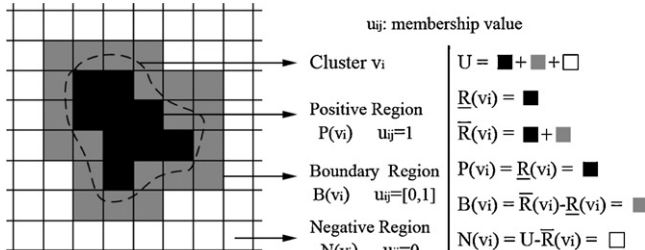


Fig. 1 – Illustration of three rough-fuzzy regions.

data in the negative region  $N(v_c)$  are definitely excluded from cluster  $c$ , and their membership to cluster  $c$  should be zero. Thus, the objective function shown in Eq. (6) can be simplified as

$$J_{GRFCM} = \lambda \sum_{c=1}^C \sum_{i \in P(v_c)} \|I_i - b_i v_c\|^2 + (1 - \lambda) \sum_{c=1}^C \sum_{i \in B(v_c)} u_{ci}^m \|I_i - b_i v_c\|^2 \quad (10)$$

It should be noted that positive regions may be empty. To avoid the sensitiveness to initializations, we assign all pixels to the boundary region  $B(v_c)$ , if the positive region  $P(v_c)$  is empty. In this case, the GRFCM algorithm would degrade to the traditional FCM algorithm.

### 3.3. Weighting parameter estimation

To balance the contribution of data from each region, both our algorithm and other improved fuzzy clustering algorithms introduce the weighting parameter  $\lambda$ . Ideally,  $\lambda$  should be adaptive to the accuracy of the estimated rough regions, taking a large value for an accurate rough region and a small value for an inaccurate region. However, the weighting parameter  $\lambda$  is set manually as a fixed value in most existing algorithms. In this paper, we used incorporated the estimation of optimal balance parameter for each cluster into solving the overall clustering problem, and proposed an iterative solution.

Obviously, an accurate estimation of the positive region  $P(v_c)$  may cover most pixels of the cluster  $c$ . On the contrary, an inaccurate  $P(v_c)$  must be much smaller, as many pixels of cluster  $c$  may lie in the boundary region. Therefore, we define the adaptive weighting parameter for each cluster as the percentage of the positive region area within the area of the entire cluster, shown as follows:

$$\lambda_c = \frac{|P(v_c)|}{|\{l_i = c; i = 1, \dots, n\}|} \quad (11)$$

where

$$l_i = \arg \max_{c=1, \dots, C} \{u_{ci}\} \quad (12)$$

is the class label of pixel  $i$  obtained according to the maximum membership.

With the estimated adaptive weighting parameters, the objective function can be re-written as

$$J_{GRFCM} = \sum_{c=1}^C \left( \lambda_c \sum_{i \in P(v_c)} \|I_i - b_i v_c\|^2 \right) + \sum_{c=1}^C \left[ (1 - \lambda_c) \sum_{i \in B(v_c)} u_{ci}^m \|I_i - b_i v_c\|^2 \right] \quad (13)$$

### 3.4. Bias field approximation

We assume that the bias field  $b$  can be approximated at the pixel-by-pixel level by using the following linear combination of orthogonal polynomials

$$b_i = \sum_{k=1}^M \omega_k g_k(i) = w^T G(i) \quad (14)$$

where  $M = (D+1)(D+1)/2$  is the number of polynomials  $g_k(i)$ ,  $w^T G(i)$  gives a linear combination of a set of basis functions  $G(i)$ , which are orthogonal polynomials in this study, and  $\{\omega_k \in \mathbb{R}, k = 1, \dots, M\}$  are real-valued combination coefficients. Theoretically, any function can be approximated by a linear combination of a set of basis functions up to arbitrary accuracy [22], and  $D$  is the degree of those polynomials.

To estimate and correct the bias field, we should determine the combination coefficients  $\omega = \{\omega_1, \omega_2, \dots, \omega_M\}$  through taking the derivative of the objective function  $J_{GRFCM}$  with respect to  $\omega$ . However, due to the utilization of weighting parameter  $\lambda$ , estimating  $\omega$  in this way becomes computationally difficult. Nevertheless, the bias field in an observed MR image has fixed values, regardless of the variation of  $\lambda$ . Therefore, we defined the following un-weighted version of the objective function to estimate  $w$

$$\tilde{J}_{GRFCM} = \sum_{c=1}^C \sum_{i \in \Omega} u_{ci}^m \|I_i - w^T G(i) v_c\|^2 \quad (15)$$

By taking the derivation of  $\tilde{J}_{GRFCM}$  with respect to  $w$ , we get

$$\begin{aligned} \frac{\partial \tilde{J}}{\partial w} &= 2 \sum_{c=1}^C \sum_{i \in \Omega} u_{ci}^m (I_i - w^T G(i) v_c) (-G(i)^T v_c) \\ &= 2 \left\{ \sum_{i \in \Omega} G(i) G(i)^T \left( \sum_{c=1}^C u_{ci}^m v_c^2 \right) \right\} w \\ &- 2 \sum_{i \in \Omega} I_i G(i) \left( \sum_{c=1}^C u_{ci}^m v_c \right) = 0 \end{aligned} \quad (16)$$

Then we can rewrite this equation as

$$Aw - B = 0 \quad (17)$$

where

$$\left\{ \begin{array}{l} A = \sum_{i \in \Omega} G(i)G(i)^T J_1(i) \\ B = \sum_{i \in \Omega} I_i G(i)J_2(i) \\ J_1(i) = \sum_{c=1}^C u_{ci}^m v_c^2 \\ J_2(i) = \sum_{c=1}^C u_{ci}^m v_c \end{array} \right. \quad (18)$$

Since the  $M \times M$  matrix  $A$  is nonsingular [22], combination coefficients  $w$  can be estimated as

$$w = A^{-1}B \quad (19)$$

### 3.5. Objective function minimization

Similar to other FCM-like algorithms, the objective function  $J_{GRFCM}$  can be minimized in an iterative way. In each step, it is minimized with respect to each variable while keeping other variables fixed. This minimization process can be summarized as follows:

1. Initialize the centroids of all clusters  $\{v_1, v_2, \dots, v_C\}$  randomly, and set the bias field to be  $b = \{1, 1, \dots, 1\}$ .
2. Determine three rough-fuzzy regions for each cluster by using Eqs. (7)–(9).
3. Calculate memberships  $\{u_{ci}; c = 1, \dots, C, i = 1, \dots, N\}$  as follows:

$$u_{ci} = \begin{cases} 1 & \text{if } I_i \in P(v_c) \\ \left\{ \sum_{k=1}^C \left[ \left( \frac{\|I_i - b_i v_k\|^2}{\|I_i - b_i v_c\|^2} \right)^{\frac{1}{m-1}} \right] \right\}^{-1} & \text{if } I_i \in B(v_c) \\ 0 & \text{if } I_i \in N(v_c) \end{cases} \quad (20)$$

4. Assign each pixel  $i$  a class label  $l_i$  according to Eq. (12).
5. Estimate the adaptive weighting parameters  $\{\lambda_1, \lambda_2, \dots, \lambda_C\}$  according to Eq. (11);
6. Update cluster centroids as follows, if either the positive region or boundary region is non-empty

$$v_c = \lambda_c \frac{\sum_{i \in P(v_c)} I_i b_i}{\sum_{i \in P(v_c)} b_i^2} + (1 - \lambda_c) \frac{\sum_{i \in B(v_c)} u_{ci}^m I_i b_i}{\sum_{i \in B(v_c)} u_{ci}^m b_i^2} \quad (21)$$

7. Otherwise, all the pixels in the image should be used in the calculation

$$v_c = \frac{\sum_{i=1}^N u_{ci}^m I_i b_i}{\sum_{i=1}^N u_{ci}^m b_i^2} \quad (22)$$

8. Approximate the bias field  $b = \{b_1, b_2, \dots, b_N\}$  by using Eqs. (14)–(19);

Repeat steps 2–7 until the total distance between the cluster centroids obtained from two successive iterations becomes smaller than a user specified threshold (0.001 is used in this paper for all the experiments).

## 4. Experiment results

We applied the proposed GRFCM algorithm to the segmentation of brain MR images into GM, WM, CSF and background. To facilitate the visions, we compared the proposed algorithm with the other relative methods on 2D brain MR images in this section. The parameters used in our experiments were set as follows. The centroids are initialized randomly and should be the different from each other. The degree of polynomials  $D$  was set to be 3, and hence the number of the basis functions  $M$  was 10. The size of the neighborhood used in defining rough-fuzzy regions was  $3 \times 3$ . And the fuzzy factor  $m$  took its default value 2.

The performance of segmenting each type of brain tissues was evaluated quantitatively by using the Dice coefficient (DC), which is defined as the ratio between the intersection and union of the obtained region  $S_1$  and ground truth region  $S_2$

$$DC(S_1, S_2) = \frac{2 |S_1 \cap S_2|}{|S_1| + |S_2|} \quad (23)$$

The value of DC ranges from 0 to 1, with a higher value representing a more accurate segmentation result.

The first experiment was performed in synthetic brain MR images selected from the Brain Web Simulated Brain Database (BrainWeb) [25]. BrainWeb provides full three-dimensional data volumes which have been simulated using three sequences (T1-, T2-, and PD-weighted) and a variety of slice thicknesses, noise levels, and levels of intensity non-uniformity. In our experiments, we use the T1-weighted 1 mm brain MR images with different level of noise and intensity inhomogeneity. Since the typical noise level in real MR data is around 3%, a synthetic brain MR image containing 3% noise and 40% INU was selected and shown in Fig. 2(a). The corresponding ground truth of brain tissues is shown in Fig. 2(b). The estimated bias field, bias corrected image and segmentation result are displayed in Fig. 2(c)–(e). Three rough-fuzzy regions for each of WM, GM and CSF are shown in Fig. 2(f)–(h), where the positive region, boundary region and negative region were illustrated in bright, gray, and dark respectively. Finally, the membership function of WM, GM and CSF are depicted in Fig. 2(i)–(k). It reveals that the proposed algorithm can construct rough-fuzzy regions appropriately, and estimate and remove the bias field effectively. Comparing Fig. 2(e) to Fig. 2(b), we found that the tissue segmentation obtained by applying our algorithm is consistent with the ground truth.

The second experiments were carried out in 3T-weighted brain MR images adapted from Ref. [22]. Three MR slices, together with the estimated bias fields, bias corrected images, and segmentation results were displayed in Fig. 3. It shows that the intensities within each brain tissue in the bias corrected images become quite homogeneous. It demonstrates

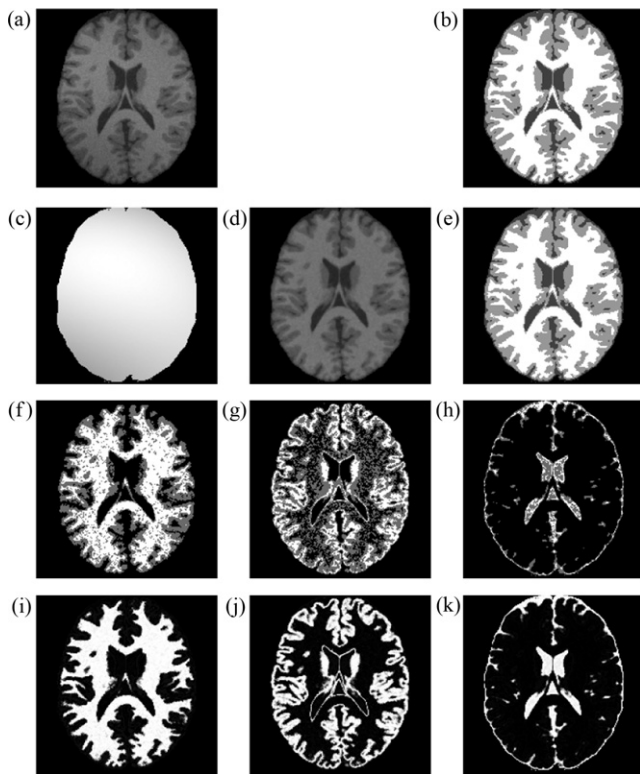


**Fig. 2 – Illustration of (a) a simulated brain MR image with 3% noise and 40% INU, (b) its segmentation ground truth, (c) the estimated bias fields, (d) bias-corrected image, (e) segmentation result of our GRFCM algorithm, (f) rough-fuzzy region of WM, (g) rough-fuzzy region of GM, (h) rough-fuzzy region of CSF, (i) membership function of WM, (j) membership function of GM, and (k) membership function of CSF.**

again that the results of our segmentation algorithm are consistent with the expected tissue regions.

To demonstrate the ability of the proposed algorithm to exempt from skull stripping, we performed the third experiment in 7 T brain MR images with skulls adapted from Ref. [7] and Ref. [26]. Fig. 4 shows two example images, the estimated bias fields, bias corrected images, and segmentation results. It is clear that the proposed algorithm can still achieve satisfying performance without being influenced by the skull.

Next, we compared the proposed segmentation algorithm to the RCM (Rough c-means) [12], RFCM (Rough fuzzy c-means) [19], RPFCM (Rough possibilistic fuzzy c-means) [20], and SCM (Shadowed c-means) [21] algorithms in simulated T1-weighted brain MR images. Since the RCM, RFCM, RPFCM and SCM algorithms cannot remove the INU from images, the test MR images selected from BrainWeb contain different level of noise, but no INU. Three example brain MR images with 9% noise, together with their segmentation results and ground truth, are shown in Fig. 5. The accuracy of all five algorithms in segmenting GM and WM from MR images with different noise levels are compared in Fig. 6. This comparison demonstrates that the proposed algorithm produce the most accuracy segmentation and has the best ability to denoise, especially in the area with abundant textures and details.

To demonstrate its ability to correct the bias field, the proposed algorithm was also compared to the methods developed by Wells et al. [4], Leemput et al. [5], Pham and Prince [8] and Li et al. [22] in synthetic brain MR images corrupted by INU. Three brain MR images with 3% noise and 100% of INU were shown in the first column of Fig. 7. The obtained segmentation results and ground truth were displayed in the rest columns. The DC values calculated in the segmentation results of 20 brain MR images were compared in Fig. 8. Those synthetic brain MR images contain 3% noise and different level of INU, ranging from 20% to 100%. Both Figs. 7 and 8 illustrate that, among those five algorithms, our algorithm

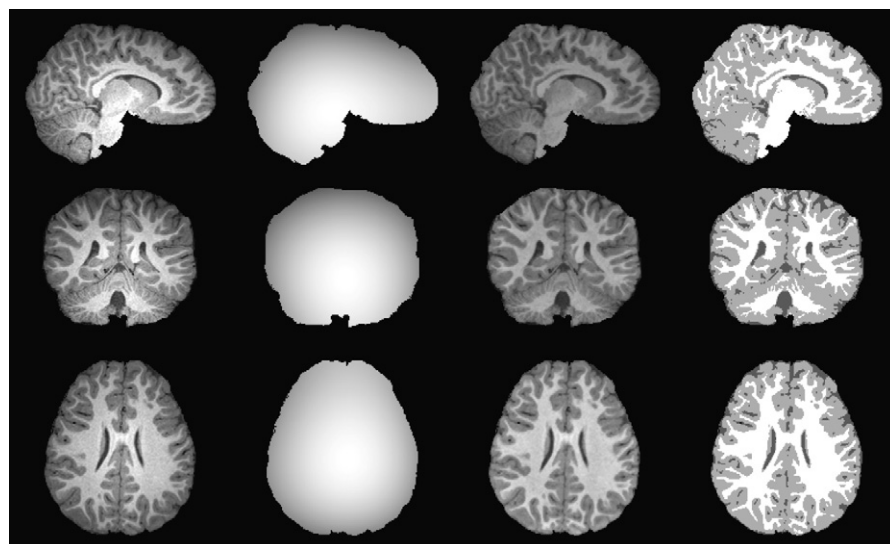


**Fig. 3 – Illustration of (1st column) three 3T-weighted brain MR images, (2nd column) their estimated bias fields, (3rd column) bias-corrected images, and (4th column) segmentation results of our GRFCM algorithm.**

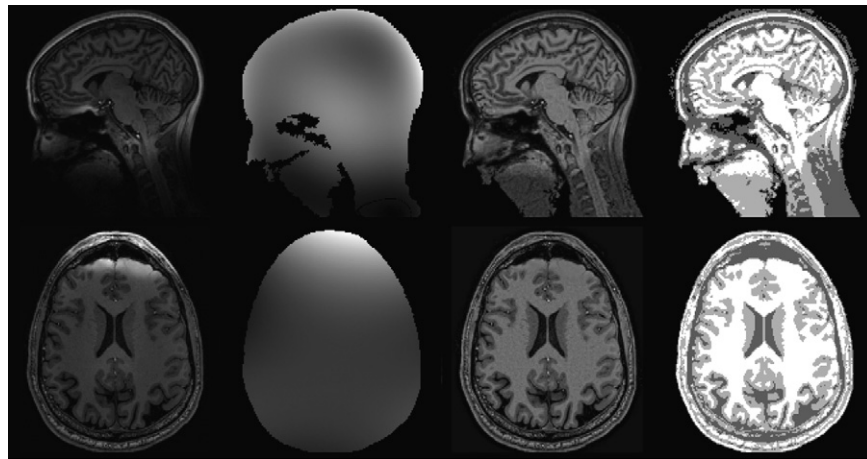


**Fig. 4 – Illustration of (1st column) two 7T-weighted brain MR images with skull, (2nd column) their estimated bias fields, (3rd column) bias-corrected images, and (4th column) segmentation results of our GRFCM algorithm.**

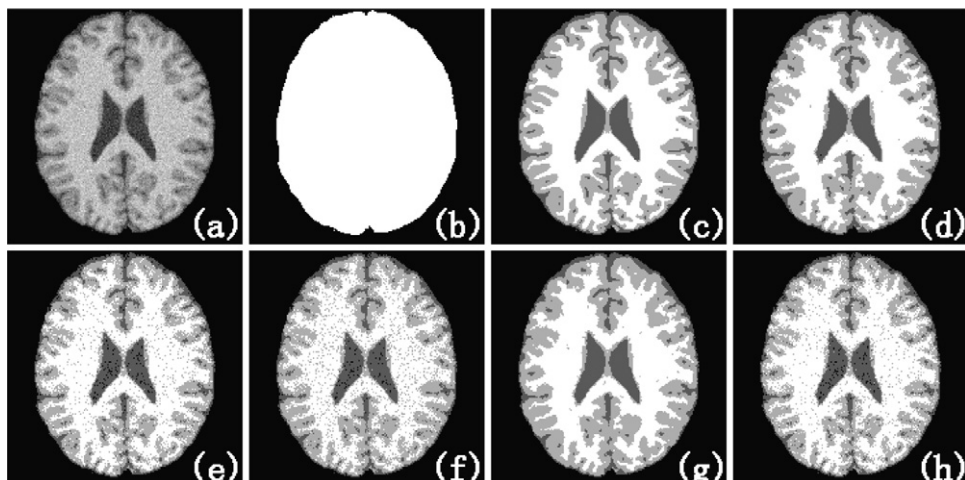


**Fig. 5 – Illustration of (a) a simulated T1-weighted brain MR images with 9% noise, (b) its brain mask, (c) segmentation ground truth, and segmentation results obtained by applying (d) the proposed GRFCM, (e) RCM, (f) RFCM, (g) RPFCM, and (h) SCM algorithms.**

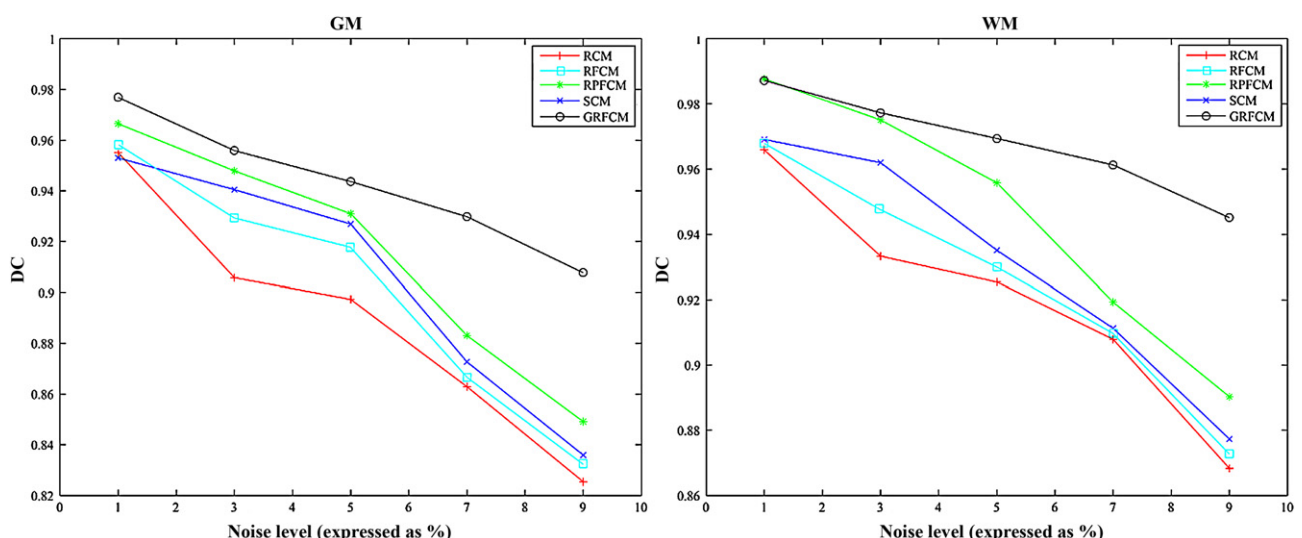


**Fig. 6 – DC values of the (left) GM and (right) WM segmentation obtained by applying five algorithms to simulated T1-weighted brain MR images with increasing level of noise.**

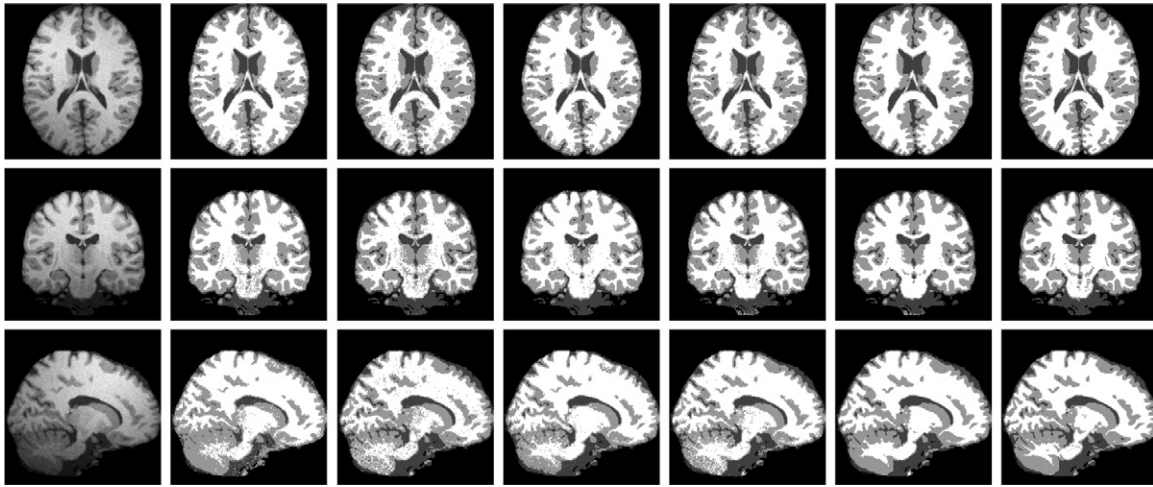


**Fig. 7 – Illustration of (1st column) three synthetic MR images with 3% noise and 100% INU, their segmentation results obtained by applying (2nd column) the method developed by Wells et al., (3rd column) method developed by Leemput et al., (4th column) method developed by Pham and Prince, (5th column) method developed by Li et al., and (6th column) the proposed GRFCM algorithm, and (7th column) the segmentation ground truth.**

can produce the most accurate segmentation of brain MR image with various levels of INU. It should be noted that we set the fuzzier  $m$  be 2 for RCM, RFCM, RPFCM, SCM and the proposed algorithm, and set the balance parameter be 0.95 for RCM, RFCM and RPFCM. Moreover, we test these five algorithms with 2D brain MR images from BrainWeb, and the average accuracy of the segmentations are calculated based on 20 different 2D brain MR images.

Further, we compared those five algorithms in clinical brain MR images selected from Ref. [27]. Four T1-weighted adult brain MRI images with 3% noise and 60–80% INU were shown in the first column of Fig. 9. The segmentation results obtained by applying three algorithms were displayed in the second, third and fourth column, respectively. The segmentation ground truth generated by medical professionals was given in the last column for visual comparison. It reveals that the proposed method outperforms other two methods in noise resistance. The DC values of the GM and WM segmentation shown in Fig. 9 were compared in Table 1. These results show

that our algorithm has the ability to improve substantially the segmentation of clinical brain MR images.

## 5. Discussion

Many fuzzy clustering algorithms are criticized for their dependence on initialization. Nevertheless, the proposed GRFCM algorithm has distinct advantages over traditional algorithms in its robustness to initialization. We applied the RPFCM, SCM and proposed algorithm on 30 brain MR images for 20 times. Each time, all algorithms are initialized randomly. The test image were selected from BrainWeb, containing 5% noise and no INU. The DC values of the GM and WM segmentation obtained in this experiment are depicted in Fig. 10. It shows that the DC values of the results from the RPFCM and SCM algorithms vary widely over different initializations. On the contrary, DC values of the results from our algorithm have no visible change. It demonstrates that

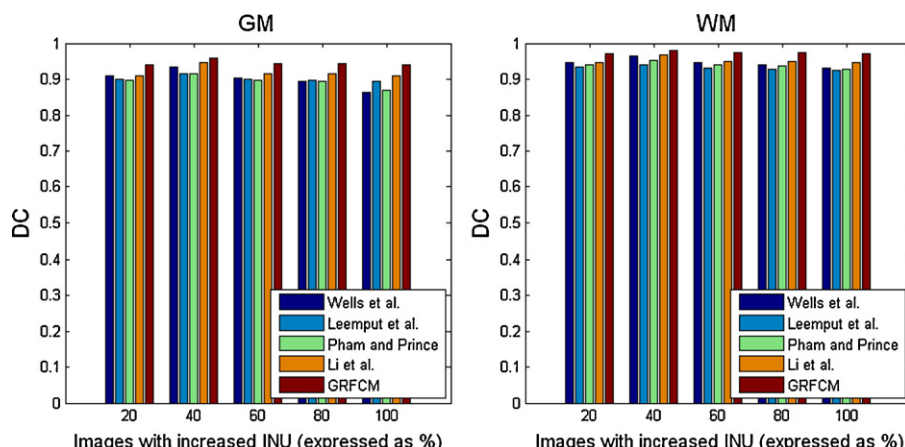


**Fig. 8 – Average DC values of the (left) GM and (right) WM segmentation obtained by applying three algorithms to 20 synthetic brain MR images with 3% noise and increasing level of INU.**

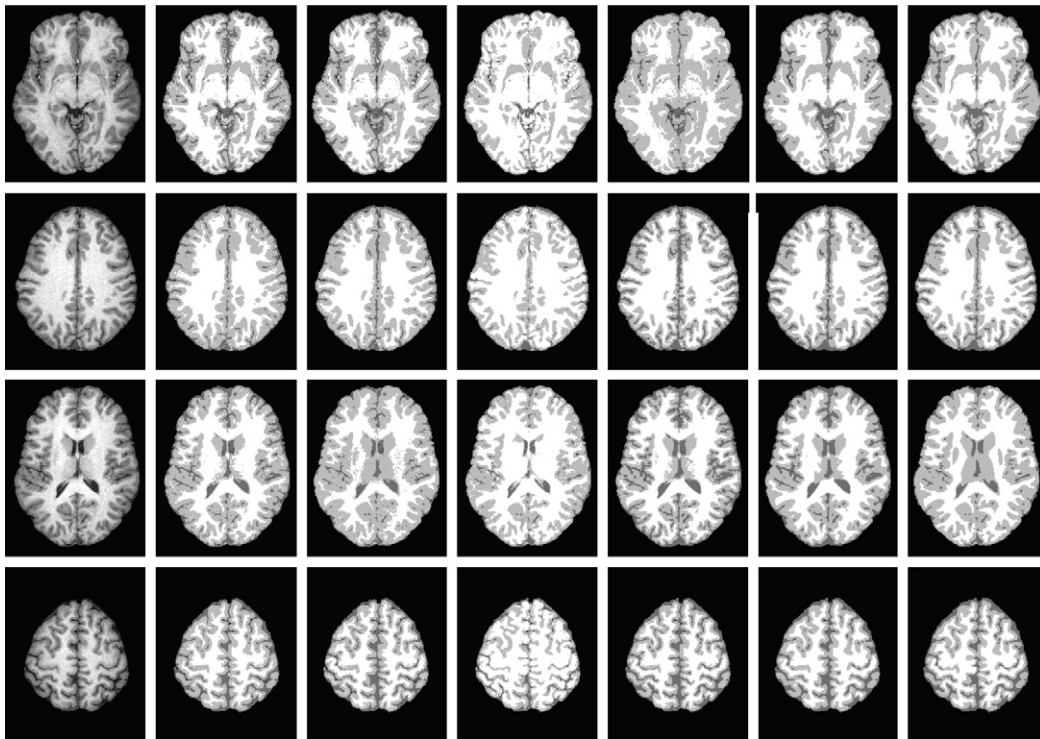


**Fig. 9 – Illustration of (1st column) four clinical MR images, their segmentation results obtained by applying (2nd column) the method developed by Wells et al., (3rd column) method developed by Leemput et al., (4th column) method developed by Pham and Prince, (5th column) method developed by Li et al., and (6th column) the proposed GRFCM algorithm, and (7th column) the segmentation ground truth.**

the accuracy of proposed segmentation algorithm is very stable and robust to initialization.

Similar to other fuzzy clustering methods, the proposed algorithm is also a continuous iterative procedure to minimize the objective function. With the automatically determined rough-fuzzy regions, our algorithm can reach an appropriate convergence very fast. To demonstrate this advantage, we

performed the segmentation of a brain MR Image 20 times, each with a random initialization. The test image is the 90th slice of the brain volume with 3% noise and 60% INU chosen from BrainWeb. Fig. 11 plots the variation of the objectives over the number of iterations. It reveals that, no matter how the segmentation is initialized, our algorithm can reach a stable convergence after 12 iterations. To make sure such

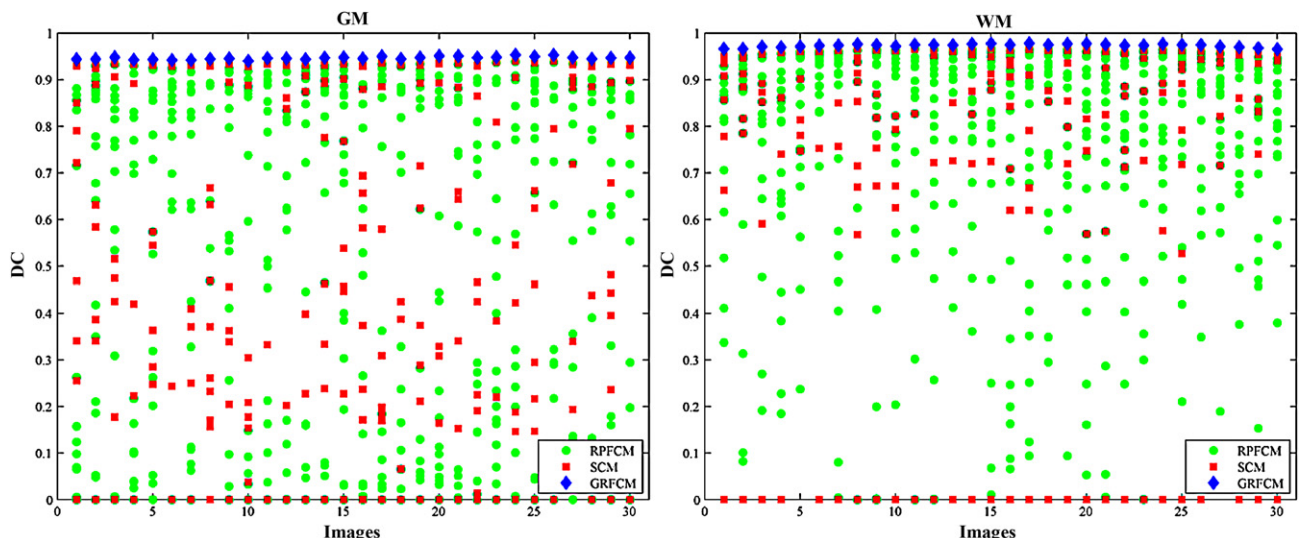


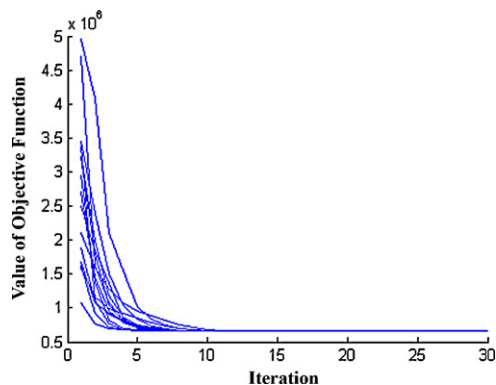
**Fig. 10 – DC values of the (left) GM and (right) WM segmentation obtained by applying the RPFM, CSM and proposed GRFCM algorithm with 20 different initializations to 30 brain MR images.**

**Table 1 – DC values of the GM and WM segmentation shown in Fig. 9.**

Image index	Tissue	Wells' method	Leemput's method	Pham's method	Li's methodss	Our method
1	GM	0.7806	0.8277	0.8307	0.8451	0.8605
	WM	0.8823	0.8912	0.8518	0.8602	0.9116
2	GM	0.8124	0.8310	0.8561	0.8960	0.9167
	WM	0.8910	0.9216	0.9075	0.9424	0.9573
3	GM	0.7833	0.8200	0.8236	0.8017	0.8979
	WM	0.8402	0.8648	0.8475	0.8703	0.8804
4	GM	0.7954	0.8044	0.8147	0.8618	0.8951
	WM	0.8446	0.8659	0.8858	0.9206	0.9246

**Table 2 – Mean ± Std of the iteration number of the proposed GRFCM algorithm when applied to 2D brain MR image segmentation.**

INU	20%	40%	60%	80%	100%	Average
Mean ± Std	10.49 ± 2.04	9.72 ± 2.06	10.16 ± 2.00	10.90 ± 2.29	10.37 ± 2.24	10.33 ± 2.96

**Fig. 11 – Convergence of the proposed GRFCM algorithm with 20 random initializations.**

efficiency does not rely on a particular image, we tested the proposed algorithm in 250 brain MR images (50 images with 20% INU, 50 images with 40% INU, 50 images with 60% INU, 50 images with 80% INU and 50 images with 100% INU). The average and standard deviation (Std) of the iterations are shown in Table 2. It reveals that the convergence of the proposed algorithm is fast and robust.

The variation of neighborhood may result in the change of segmentation results. Generally, a larger neighborhood contains more information, and has better ability to resist noise. Nevertheless, the enlargement of neighborhood may increase the risk of over-smooth boundaries and destroy the details in an image. Hence, using larger neighborhood may increase

the time-cost, but not necessarily the accuracy, of image segmentation. To our knowledge, so far, there is no universally accepted method to determine the optimal neighborhood. In this paper, we evaluated the performance of the neighborhood with the size of  $3 \times 3$ ,  $5 \times 5$ ,  $7 \times 7$ ,  $9 \times 9$  and  $11 \times 11$  in 20 2D brain MR images. Table 3 shows the estimated thresholds and segmentation accuracy obtained by using those five different types of neighborhood. It reveals that that, with the enlargement of the neighborhood, two thresholds increase only slightly, and the accuracy of segmenting GM, WM and CSF does not increase accordingly. On the contrary, the lowest DC values of the segmentation were recorded when the largest neighborhood was used. The results of this experiment also show that our method can produce reliable and relatively stable thresholds and segmentation results. To balance the computational complexity and the segmentation accuracy, in this work we empirically chose the  $3 \times 3$  neighborhood for all 2D images and  $3 \times 3 \times 3$  neighborhood for 3D images.

To evaluate its computational complexity, the proposed algorithm was tested in 40 2D and 30 3D images selected from the BrainWeb dataset [25] and IBSR [28]. The mean and standard deviation of the time cost of our algorithm in this experiment (Intel Core 2 2.66 GHz Processor, 2G Memory and Matlab Version 7.1) were listed in Table 4. It shows that our algorithm is a bit time consuming, especially when applying to large 3D image volumes. The high complexity of our algorithm is largely caused by its iterative nature and repeated bias field estimation.

It should be noted that since we adopted the orthogonal polynomials as the basis function for bias field approximation, the bias field must be smooth and very slowly. Otherwise, our

**Table 3 – Mean ± Std of the estimated thresholds used in our GRFCM algorithm and the corresponding segmentation accuracy obtained by using different size of neighborhood.**

	Size of neighborhood					Average
	$3 \times 3$	$5 \times 5$	$7 \times 7$	$9 \times 9$	$11 \times 11$	
Threshold 1	0.0341 ± 0.0004	0.0501 ± 0.0005	0.0625 ± 0.0005	0.0726 ± 0.0005	0.0810 ± 0.0005	0.0601 ± 0.0167
Threshold 2	0.2774 ± 0.0014	0.2816 ± 0.0014	0.2853 ± 0.0013	0.2887 ± 0.0012	0.2919 ± 0.0012	0.2850 ± 0.0053
DC for GM	0.9592 ± 0.0020	0.9591 ± 0.0022	0.9590 ± 0.0020	0.9590 ± 0.0020	0.9585 ± 0.0021	0.9589 ± 0.0021
DC for WM	0.9749 ± 0.0066	0.9748 ± 0.0067	0.9748 ± 0.0066	0.9746 ± 0.0068	0.9747 ± 0.0066	0.9748 ± 0.0065
DC for CSF	0.9667 ± 0.0039	0.9667 ± 0.0039	0.9665 ± 0.0039	0.9666 ± 0.0041	0.9659 ± 0.0039	0.9665 ± 0.0039

**Table 4 – Mean ± Std of the time cost of the proposed GRFCM algorithm.**

Dimension	Dataset	Number of images	Image size	Time (s)
2D	BrainWeb	20	181 × 217	18.00 ± 0.30
	IBSR	20	256 × 256	30.29 ± 0.29
3D	BrainWeb	10	181 × 217 × 181	668.60 ± 7.15
	IBSR	20	256 × 256 × (60–65)	328.77 ± 4.87

algorithm may fail to estimate and eliminate the bias field. In our experiments, we run the proposed segmentation algorithm over 500 times in 2D brain MR image, and over 40 times in 3D brain MR images (20 images are from BrainWeb and 20 from IBSR). Our algorithm work very well on simulated MR images, 3T MR images and the real MR images from Brain-Maps, but less well in 7T MR images. The reason lies in the fact that the intensity inhomogeneity is so severe in 7T brain MR images and the bias field does not follow the assumption of slow variation in the entire image domain, as shown in Fig. 4. In this case, our method cannot obtain satisfying thresholds for determining rough regions based on randomly initialized mean value of each cluster, and thus may fail to correct the bias field and result in less accurate segmentation.

## 6. Conclusion

In this paper, we propose the GRFCM algorithm, which is a novel hybrid clustering approach combining the rough c-mean and fuzzy c-mean techniques. This algorithm successfully overcomes the drawbacks of existing rough-fuzzy clustering algorithms, including semi-automated determination of rough-fuzzy regions, sensitiveness to initialization, and limited accuracy. It has been applied to the segmentation of synthetic and clinical brain MR images into GM, WM, CSF and background. Our results show that the proposed algorithm is robust to noise, bias fields and initializations, and hence can produce accurate brain MR image segmentation.

## Acknowledgements

This work was supported in part by the PolyU and ARC grants, in part by the National Natural Science Foundation of China under Grant 60773172 and Grant 60805003, in part by the National Science Foundation of Jiangsu Province under Grant BK2008411, and in part by the Doctoral Fund of Ministry of Education of China (RFDP) under Grant 200802880017.

## REFERENCES

- [1] S. Awate, T. Tasdizen, N. Foster, R. Whitaker, Adaptive Markov modeling for mutual-information-based unsupervised MRI brain-tissue classification, *Med Image Anal.* 10 (5) (2007) 726–739.
- [2] W. Wong, A. Chung, Bayesian image segmentation using local iso-intensity structural orientation, *IEEE Trans Image Process.* 14 (10) (2005) 1512–1523.
- [3] U. Vovk, F. Pernus, B. Likar, A review of methods for correction of intensity inhomogeneity in MRI, *IEEE Trans. Med. Imaging* 26 (3) (2007) 405–421.
- [4] W. Wells, E. Grimson, R. Kikinis, F. Jolesz, Adaptive segmentation of MRI data, *IEEE Trans. Med. Imaging* 15 (4) (1996) 429–442.
- [5] K. Van Leemput, K. Maes, D. Vandermeulen, P. Suetens, Automated model-based bias field correction of MR images of the brain, *IEEE Trans. Med. Imaging* 18 (10) (1999) 885–896.
- [6] Y. Zhang, M. Brady, S. Smith, Segmentation of brain MR images through a hidden Markov random field model and the expectation–maximization algorithm, *IEEE Trans. Med. Imaging* 20 (1) (2001) 45–57.
- [7] C.M. Li, C. Xu, A. Anderson, J. Gore, MRI tissue classification and bias field estimation based on coherent local intensity clustering: a unified energy minimization framework, *information processing in medical imaging (IPMI), Lect. Notes Comput. Sci.* 5636 (2009) 288–299.
- [8] D. Pham, J. Prince, Adaptive fuzzy segmentation of magnetic resonance images, *IEEE Trans. Med. Imaging* 18 (9) (1999) 737–752.
- [9] M.N. Ahmed, S. Yamany, N. Mohamed, A.A. Farag, T. Moriarty, A modified fuzzy c-means algorithm for bias field estimation and segmentation of MRI data, *IEEE Trans. Med. Imaging* 21 (3) (2002) 193–199.
- [10] A.W.C. Liew, H. Yan, An adaptive spatial fuzzy clustering algorithm for 3-D MR image segmentation, *IEEE Trans. Med. Imaging* 22 (9) (2003) 1063–1075.
- [11] J.C. Bezdek, *Pattern Recognition with Fuzzy Objective Function Algorithms*, Kluwer Academic Publishers, Norwell, MA, USA, 1981.
- [12] P. Lingras, C. West, Interval set clustering of web users with rough k-means, *Dept. Math. Comput. Sci., St. Mary's Univ., Halifax, NS, Canada, Tech. Rep. No. 2002-002*, 2002.
- [13] M.M. Mushrif, A.K. Ray, Color image segmentation: rough-set theoretic approach, *Pattern Recogn. Lett.* 29 (2008) 483–493.
- [14] S.K. Pal, P. Mitra, Multispectral image segmentation using rough set initialized EM algorithm, *IEEE Trans. Geosci. Rem. Sens.* 40 (2002) 2495–2501.
- [15] S. Widz, D. Slezak, Approximation Degrees in Decision Reduct-Based MRI Segmentation, in: *Proceedings of the Frontiers in the Convergence of Bioscience and Information Technologies*, 2007, pp. 431–436.
- [16] Z. Pawlak, *Rough Sets, Theoretical Aspects of Reasoning About Data*, Kluwer, Dordrecht, The Netherlands, 1991.
- [17] D. Dubois, H. Prade, Rough fuzzy sets and fuzzy rough sets, *Int. J. Gen. Syst.* 17 (1990) 191–209.
- [18] D. Dubois, H. Prade, Putting fuzzy sets and rough sets together, in: R. Slowinski (Ed.), *Intelligent Decision Support*, 1992, pp. 203–232.
- [19] P. Maji, S.K. Pal, RFCM: a hybrid clustering algorithm using rough and fuzzy sets, *Fundam. Inform.* 79 (2007) 1–22.
- [20] P. Maji, S.K. Pal, Rough set based generalized fuzzy c-means algorithm and quantitative indices, *IEEE Trans. Syst. Man Cybernet. B Cybernet.* 37 (2007) 1529–1540.
- [21] S. Mitra, W. Pedrycz, B. Barman, Shadowed c-means: integrating fuzzy and rough clustering, *Pattern Recogn.* 43 (4) (2009) 1282–1291.
- [22] C.M. Li, C. Gatenby, L. Wang, J. Gore, A robust parametric method for bias field estimation and segmentation of MR images, in: *Proceedings of IEEE Conference on Computer*

- Vision and Pattern Recognition (CVPR), vol. 21, 2009, pp. 8–223.
- [23] S. Hirano, S. Tsumoto, Rough representation of a region of interest in medical images, *Int. J. Approx. Reason.* 40 (2005) 23–34.
- [24] Z.X. Ji, Q.S. Sun, D.S. Xia, P.A. Heng, MR Image Segmentation with Generalized Rough Fuzzy c-means Algorithm, *Proceedings of the third International Workshop on Image Analysis, IWIA2010*, Nimes, France. Achevé d'imprimer en 2011. ISBN: 978-2-911256-55-4. (2011) 203–212.
- [25] Brainweb, Simulated Brain Database.  
<http://www.bic.mni.mcgill.ca/brainweb/>.
- [26] Y.J. Chen, J.W. Zhang, J. Macione, An improved level set method for brain MR images segmentation and bias correction, *Comput. Med. Imaging Graph.* 33 (5) (2009) 510–519.
- [27] L. Wang, Y.J. Chen, X.H. Pan, H. XN, D.S. Xia, Level set segmentation of brain magnetic resonance images based on local Gaussian distribution fitting energy, *J. Neurosci. Methods* 188 (2) (2010) 316–325.
- [28] IBSSR, The Internet Brain Segmentation Repository.  
<http://www.cma.mgh.harvard.edu/ibsr/>.